Numerical evidence of the double-Griffiths phase of the random quantum Ashkin-Teller chain

Christophe Chatelain, Dimitrios Voliotis

EPJ manuscript No.
(will be inserted by the editor)

Numerical evidence of the double-Griffiths phase of the random quantum Ashkin-Teller chain

C. Chatelain and D. Voliotis

Groupe de Physique Statistique, Département P2M, Institut Jean Lamour (CNRS UMR 7198), Université de Lorraine, France
e-mail: christophe.chatelain@univ-lorraine.fr

the date of receipt and acceptance should be inserted later

Abstract. The random quantum Ashkin-Teller chain is studied numerically by means of time-dependent Density-Matrix Renormalization Group. The critical lines are estimated as the location of the peaks of the integrated autocorrelation times, computed from spin-spin and polarization-polarization autocorrelation functions. Disorder fluctuations of magnetization and polarization are observed to be maximum on these critical lines. Entanglement entropy leads to the same phase diagram, though with larger finite-size effects. The decay of spin-spin and polarization-polarization autocorrelation functions provides numerical evidence of the existence of a double Griffiths phase when taking into account finite-size effects. The two associated dynamical exponents z increase rapidly as the critical lines are approached, in agreement with the recent conjecture of a divergence at the two transitions in the thermodynamic limit.

PACS. 05.30.Rt Quantum phase transitions – 05.70.Jk Critical point phenomena – 05.10.-a Computational methods in statistical physics and nonlinear dynamics

1 Introduction

Classical and quantum phase transitions are affected differently by the introduction of homogeneous disorder. In the former, it is well established that, when no frustration is induced, disorder is a relevant perturbation at a critical point when thermal fluctuations grow slower than disorder ones inside the correlation volume. It follows that the critical behavior is unchanged when the specific heat exponent α of the pure model is negative [1]. This criterion, due to Harris, has been extensively tested on classical toy models such as the 2D Ashkin-Teller model [2] or the 2D q-state Potts model [3,4]. In the latter, disorder is relevant for $q > 2$ and the new random fixed point depends on the number of states q.

Quantum phase transitions, i.e. transitions driven by quantum fluctuations rather than thermal ones, involve new phenomena. First, randomness can never be considered as homogeneous because time plays the role of an additional dimension. Therefore, in contrast to the classical case, even when random couplings are homogeneously distributed on the lattice, they are always infinitely correlated in the time direction. Indeed, the random quantum Ising chain in a transverse field (RTFIM), for instance, is equivalent to the celebrated McCoy-Wu model, a classical 2D Ising model with couplings that are randomly distributed in one direction but perfectly correlated in the second one [5,6]. As a consequence, scale invariance is broken even after averaging over disorder. The random quantum fixed point is usually invariant under anisotropic scaling transformations. Correlation length ξ and autocorrelation time ξ_t grow differently when approaching the random quantum critical point:

$$\xi_t \sim \xi^z, \tag{1}$$

where z is the dynamical exponent. In the RTFIM, or in any model whose critical behavior is described by the same fixed point, this dynamical exponent increases algebraically when approaching the critical point and diverges at the critical point.

Another feature of quantum phase transitions in presence of disorder is the existence of Griffiths phases [7]. In the paramagnetic phase, there may exist large regions with a high concentration of strong couplings which can therefore order ferromagnetically earlier than the rest of the system. Even though the probability of such regions is exponentially small, they can cause a singular behavior of the free energy with respect to the magnetic field in a finite range of values of the quantum control parameter. The region of the paramagnetic phase where this phenomena occurs is called a disordered Griffiths phase. A similar phenomena takes place in the ferromagnetic phase. The singular behavior is due to regions of the system with a high concentration of weak bonds at their boundaries. They are therefore only weakly coupled to the rest of the system and can order independently [8]. Because the tunneling time of these rare regions grows exponentially fast with their size, they have a drastic effect on the aver-

age autocorrelation functions of the system. Instead of the usual exponential decay, the latter displays an algebraic decay [11]

$$\overline{A(t)} \sim t^{-1/z} \tag{2}$$

involving the dynamical exponent z. In classical systems, Griffiths phases usually consist in essential singularities, too weak to be observed numerically, apart with some long-range correlated disorder [9,10].

The quantum Ising chain in a transverse magnetic field has been, by far, the most studied system undergoing a quantum phase transition. The mapping of this model onto a lattice gas of free fermions allowed for exact calculations in the pure case [12]. In the presence of random couplings, exact results are sparse [13] but the mapping still allows for an efficient numerical estimate of static, as well as dynamic, quantum averages [14]. The critical behavior is governed by an unusual infinite-randomness fixed point (IRFP) which has been extensively studied using a real-space renormalization group approach, the Strong-Disorder Renormalization Group (SDRG), first introduced by Ma and Dasgupta [15], and later extended to the RTFIM by Fisher [16–18]. The strongest coupling, exchange interaction or transverse field, is decimated by projecting out the Hilbert space onto the ground state of this coupling. Other couplings are then treated using second-order perturbation theory. Nevertheless, the method is believed to become exact as the IRFP is approached because the probability distribution of random couplings becomes broader and broader and therefore, a strong coupling is always surrounded by weaker couplings that can be treated perturbatively. The dynamical exponent z was shown to diverge at the phase transition. The relation (1) is replaced by $\xi \sim (\ln \xi_t)^{1/\psi}$ with $\psi = 1/2$. Autocorrelation functions decay as [19]

$$\overline{A(t)} \sim (\ln t)^{-2x_\sigma} \tag{3}$$

at the critical point, while correlation functions $C(r)$ display a more usual algebraic decay with the distance r. The Ma-Dasgupta renormalization group allows for the exact determination of the magnetization scaling dimension and the correlation length exponent [16,17]:

$$2x_\sigma = 2\beta/\nu = 2 - \frac{1+\sqrt{5}}{2}, \quad \nu = 1/\psi = 2. \tag{4}$$

The approach has been applied numerically to higher dimensions [20–22]. The IRFP of the RTFIM is quite robust: in contrast to the classical case, the random quantum q-state Potts chain falls also into this universality class for any value of q [23,24].

In this paper, a model with a richer phase diagram is considered. The quantum two-color Ashkin-Teller model can be seen as two coupled Ising chains in a transverse field. The Hamiltonian is [27]

$$H = -\sum_i \left[J_i \sigma_i^z \sigma_{i+1}^z + h_i \sigma_i^x\right] - \sum_i \left[J_i \tau_i^z \tau_{i+1}^z + h_i \tau_i^x\right] - \sum_i \left[K_i \sigma_i^z \sigma_{i+1}^z \tau_i^z \tau_{i+1}^z + g_i \sigma_i^x \tau_i^x\right] \tag{5}$$

where $\sigma_i^{x,y,z}$ and $\tau_i^{x,y,z}$ are two sets of Pauli matrices. The model possesses two $\mathbb{Z}_2$-symmetries, corresponding to the invariance of the Hamiltonian under the reversal of all spins σ_i (or τ_i) and of both σ_i and τ_i. The breaking of these symmetries can be monitored using the two order parameters

$$M = \sum_i \langle \sigma_i^z \rangle, \quad P = \sum_i \langle \sigma_i^z \tau_i^z \rangle \tag{6}$$

referred to as magnetization and polarization. In the pure case, i.e. $J_i = J$, $K_i = K$, $h_i = h$ and $g_i = g$, the phase diagram involves several critical lines, as the 2D classical Ashkin-Teller model [25,26,28,29]. When $K < J$, the two $\mathbb{Z}_2$ symmetries are simultaneously broken and the Ashkin-Teller model undergoes a single second-order quantum phase transition with the control parameter $\delta = J/h$. The scaling dimensions of magnetization, polarization and energy densities vary along the critical line [27]:

$$x_\sigma = \frac{1}{8}, \; x_{\sigma\tau} = \frac{\pi}{8\arccos(-\epsilon)}, \; x_\varepsilon = \frac{\pi}{2\arccos(-\epsilon)} \tag{7}$$

for $\epsilon = K/J \in [-1/\sqrt{2}; 1]$. For $K > J$, i.e. $\epsilon > 1$, the critical line splits into two lines, both belonging to the Ising universality class ($x_\sigma = 1/8$, $x_{\sigma\tau} = x_{\sigma^2} = 1/16$ and $x_\varepsilon = 1$). These lines separate the paramagnetic ($M = P = 0$) and Baxter ($M, P \neq 0$) phases from an intermediate mixed phase ($M = 0$, $P \neq 0$).

In the following, the random Ashkin-Teller chain is considered. The four couplings J_i, h_i, K_i and g_i are random variables, though not independent but constrained by the relation [1]

$$\frac{K_i}{J_i} = \frac{g_i}{h_i} = \epsilon \tag{8}$$

where ϵ is a site-independent fixed parameter. This model was first studied numerically by means of Density-Matrix Renormalization Group (DMRG) in the weak-disorder regime $\epsilon < 1$ [30]. As in the pure model, the system undergoes a single quantum phase transition with the control parameter

$$\delta = \overline{\ln J} - \overline{\ln h}. \tag{9}$$

SDRG shows that the inter-chain couplings K_i and g_i are irrelevant on the critical line $\delta = 0$, i.e. the random Ashkin-Teller model behaves as two uncoupled random Ising chains. The critical behavior is therefore governed by the Fisher infinite-randomness fixed point with the critical exponents (4). However, for finite disorder strength, a strong cross-over is observed numerically between the pure

[1] The case where $K_i/J_i = \epsilon_J$ and $g_i/h_i = \epsilon_h$ are different was considered in [31]. At the infinite-randomness fixed point, both quantities are renormalized to the same value, $\epsilon^* = 0$ in the weak-coupling regime ($\epsilon_J, \epsilon_h < 1$) and $\epsilon \to +\infty$ in the strong-coupling one. Without loss of generality, one can start with $\epsilon_J = \epsilon_h$. The more general case where ϵ_J and ϵ_h are random variables and are allowed to take values both above and below 1 was also considered in [31] and leads to a different critical behavior at the multicritical point.

fixed point and this infinite-randomness fixed point. The regime $\epsilon > 1$ of the random Ashkin-Teller model was only studied more recently using SDRG [31,32]. The phase diagram is qualitatively the same as the pure Ashkin-Teller model, in particular the two Ising lines still meets at a tricritical point located at $\delta = 0$ and $\epsilon = 1$. When this point is approached by varying δ, the scaling dimensions (4) of the infinite-randomness Ising fixed point are recovered. However, when approaching this point along the half-line $\delta = 0$ and $\epsilon > 1$, the critical behavior is governed by different exponents:

$$\beta = \frac{6 - 2\sqrt{5}}{1 + \sqrt{7}}, \quad \nu = \frac{8}{1 + \sqrt{7}}. \tag{10}$$

Note that the ratio β/ν is unchanged, a property sometimes referred to as weak universality. Between the two Ising lines in the regime $\epsilon > 1$, SDRG indicates the existence of a double Griffiths phase: magnetization behaves as in the disordered Griffiths phase of the random Ising chain but polarization as in the ordered Griffiths phase.

In the rest of the paper, new data of both regimes $\epsilon < 1$ and $\epsilon > 1$ obtained by DMRG are presented and discussed. While only the critical point was considered in [30], we are interested in the out-of-critical region of the phase diagram and especially in the Griffiths phases when $\epsilon > 1$. In the first section, details about the implementation of the model and the parameters used for numerical computations are presented. In the second section, the phase boundaries are determined using integrated autocorrelation times, and the disorder fluctuations of magnetization and polarization. They are compared with the behavior of the entanglement entropy of one half of the lattice with the rest of the system. In the third section, the spin-spin and polarization-polarization autocorrelation functions are analyzed more carefully. In particular, we are interested in the algebraic decay (2) signaling the existence of a Griffiths phase. Finally, a conclusion follows.

2 Numerical details

We have considered a binary distribution of the intra-chain couplings J_i:

$$\wp(J_i) = \frac{1}{2}\big[\delta(J_i - J_1) + \delta(J_i - J_2)\big] \tag{11}$$

and homogeneous transverse fields h and g. Equation (8) now reads

$$\frac{K_i}{J_i} = \frac{g}{h} = \epsilon. \tag{12}$$

The critical behavior is expected to be unaffected by this choice. Indeed, the probability distributions of h and g, initially delta peaks, will become broader and broader under renormalization so that the same IRFP will be eventually reached. This choice was made to minimize the number of disorder configurations. If L is the lattice size, the number of J_i couplings is $L - 1$ with open boundary conditions so the total number of disorder configurations is 2^{L-1}. For small lattice sizes, up to $L = 16$, the average over disorder can be performed exactly and the possibly disastrous consequences of an under-sampling of rare events can be avoided [33]. This strategy is motivated by the fact that we are mainly interested in Griffiths phases, where the dominant behavior is due to rare disorder configurations. The drawback is that a precise determination of critical exponents is more difficult, in contrast to [30] where the sampling was limited to 10,000 disorder configurations, allowing for larger lattice sizes up to $L = 32$. We also made additional calculations for a lattice size $L = 20$ but with an average over only 50,000 disorder configurations, randomly chosen among the 524,288 ones. As we will see, this under-sampling leads to observable deviations.

For simplicity, we have moreover restricted ourselves to the case

$$J_2 = 1/J_1 \;\Leftrightarrow\; \overline{\ln J_i} = 0. \tag{13}$$

and we have chosen a strong disorder by setting $J_1 = 4$ and $J_2 = 1/4$. The quantum control parameter is now

$$\delta = -\ln h. \tag{14}$$

The model was studied using the time-dependent Density-Matrix Renormalization Group algorithm [34–36]. A rough estimate of the ground state is first obtained with the so-called Infinite-Size DMRG algorithm. Because the couplings are inhomogeneous, the system was grown by adding single spins to one boundary rather than inserting them between the two blocks. After this initial Infinite-Size step, the accuracy of the ground state is improved by performing four sweeps of the Finite-Size algorithm. Since disorder fluctuations dominate at the IRFP, quantum fluctuations are expected to be much weaker than in the pure Ashkin-Teller model. For the latter, the expected critical exponents were recovered by keeping of the order of $m = 192$ states when truncating the Hilbert space of a left or right block in the DMRG algorithm. For the random Ashkin-Teller model, we fixed the upper limit of this parameter to $m = 64$. The actual number of states was determined dynamically by imposing a maximal truncation error: 10^{-5} during the initial Infinite-Size step, 10^{-6}, 10^{-7}, 10^{-8}, and 10^{-9} during the four Finite-Size sweeps. Using these parameters, we were able to make calculations for a large number of quantum control parameters δ for lattice sizes up to $L = 20$ for $\epsilon > 1$. Unfortunately, the Arpack library, used to determine the ground-state in the truncated Hilbert space, sometimes failed for some particular disorder configurations. In these cases, the point, and not simply this disorder configuration, is discarded. For $\epsilon \leq 1$, many calculations failed for $L = 16$. Only 27 values of the control quantum parameter could be completed for $\epsilon = 1$, mostly far from the critical point. Moreover, when successful, the computation takes a time which increases very fast for $\epsilon < 1$. Since the two Ising chains are uncoupled at the fixed point, the Hilbert space becomes closer to

a tensor product of the spaces of two Ising chains. Therefore, the number of states to be kept during the truncation process of the DMRG algorithm should be of the order of the square of the number of states necessary for a single Ising chain. For this reason, the largest lattice size considered in the regime $\epsilon < 1$ is only $L = 12$.

Average magnetization and polarization densities

$$\overline{\langle m\rangle} = \overline{\langle 0|\sigma^z_{L/2}|0\rangle}, \quad \overline{\langle p\rangle} = \overline{\langle 0|\sigma^z_{L/2}\tau^z_{L/2}|0\rangle}, \tag{15}$$

were measured at the center of the chain. $|0\rangle$ denotes the ground state and the over-line bar stands for the average over disorder. In order to measure non-vanishing averages, longitudinal magnetic and electric fields were coupled to the two boundary spins of the chain with the Hamiltonian

$$H_1 = B\sigma^z_1 + E\sigma^z_1\tau^z_1 + B\sigma^z_L + E\sigma^z_L\tau^z_L \tag{16}$$

to break the two $\mathbb{Z}_2$ symmetries. The convergence of the DMRG algorithm is also faster when such boundary fields are imposed. Spin-spin and polarization-polarization connected autocorrelation functions, defined as

$$\begin{aligned}\overline{A_\sigma(t)} &= \overline{\langle 0|\sigma^z_{L/2}(t)\sigma^z_{L/2}(0)|0\rangle} - \overline{\langle m\rangle^2}, \\ \overline{A_{\sigma\tau}(t)} &= \overline{\langle 0|\sigma^z_{L/2}(t)\tau^z_{L/2}(t)\sigma^z_{L/2}(0)\tau^z_{L/2}(0)|0\rangle} - \overline{\langle p\rangle^2},\end{aligned} \tag{17}$$

were estimated using a discretized imaginary-time evolution operator:

$$\overline{A_\sigma(n\Delta t)} = \overline{\left[\frac{\langle 0|\sigma^z_{L/2}\big(1-H\Delta t\big)^n\sigma^z_{L/2}|0\rangle}{\langle 0|\big(1-H\Delta t\big)^n|0\rangle}\right]} - \overline{\langle m\rangle^2}. \tag{18}$$

We have used the value $\Delta t = 10^{-3}$ and computed autocorrelation functions up to $t = 10$.

3 Phase boundaries

As discussed in the introduction, the random quantum Ashkin-Teller model is expected to undergo a single transition when $\epsilon \leq 1$ and two transitions when $\epsilon > 1$. This is easily observed on the behavior of magnetization and polarization, which are the two order parameters of these two transitions. As seen on figures 1, magnetization and polarization display a fast variation but at different values of the transverse field h, and therefore of the control parameter $\delta = -\ln h$, when $\epsilon > 1$.

However, because of the finite-size of the system, magnetization and polarization curves are too smooth to provide accurate estimates of the location of the transitions. Diverging quantities are more convenient for that purpose and usually preferred in numerical studies. In this section, we discuss three quantities that diverge, or display a pronounced peak, at the transitions of the random Ashkin-Teller model.

3.1 Integrated autocorrelation time

One of the properties that define criticality is that any characteristic length or time disappears at a second-order phase transition. Out-of-criticality, the exponential decay of average spatial correlation functions $C(r)$ and autocorrelation functions $A(t)$ provides respectively a correlation length ξ and an autocorrelation time ξ_t. In a pure system, both quantities are expected to diverge as a critical point is approached. In the random case, a divergence of ξ and ξ_t is expected in the whole Griffiths phase. However, in a finite system, these divergences are smoothed and replaced by a finite peak. At large time t, connected autocorrelation functions $\overline{A(t)}$ are dominated by an exponential decay of the variable t/ξ_t. Consequently, their integrals behave as

$$\tau = \int_0^{+\infty} \overline{A(t/\xi_t)}dt = \xi_t \int_0^{+\infty} \overline{A(u)}du \tag{19}$$

and, like ξ_t, should display a peak. We have computed the integrated autocorrelation time τ for spin-spin and polarization-polarization autocorrelation functions. The upper bound of the integral (19) was replaced by the largest time $t = 10$ considered. This approximation has no effect on the estimate of the autocorrelation time τ as long as ξ_t is much smaller than 10. As will be seen below, this is the case for the lattice sizes that we considered.

As can be seen on figures 2 and 3, the integrated autocorrelation times display two peaks. The first peak occurs at a value of the transverse field h which is of the same order of magnitude as J_2. Therefore, this peak is probably associated to the ordering transition of the disorder configurations with a majority of weak couplings J_2. However, the height of this peak does not increase significantly with the lattice size so one can conjecture that this peak will remain finite in the thermodynamic limit and is not associated to any phase transition. The height of the second peak clearly increases with the lattice size. For $\epsilon \leq 1$, the location of the peak is roughly the same for spin-spin and polarization-polarization autocorrelation times. For $\epsilon > 1$, the data clearly shows that the peak occurs at a positive control parameter δ, i.e. a transverse field $h < 1$, for spin-spin autocorrelation functions and negative for polarization-polarization ones. This indicates that the system undergoes an electric phase transition followed, at larger control parameter, by a magnetic one. This is consistent with the picture given by magnetization and polarization curves. The location of the two transitions was predicted by Hrahsheh *et al.* to be $\delta_c = \pm\ln\frac{\epsilon}{2}$ for $\epsilon \gg 1$ [31]. For $\epsilon = 4$, we observe the two peaks at $\delta_c = -\ln h_c \simeq 0.54$ and $\delta_c \simeq -0.99$ for $L = 16$ for instance, still far from $\pm\ln\frac{\epsilon}{2} \simeq \pm 0.69$. Moreover, our transitions lines are not symmetric with respect to the axis $\delta = 0$, as required by self-duality. Since the data was produced by DMRG with a relatively large number of states and since the averages were made over all disorder configurations, the deviation can only be the consequence of the relatively small lattice sizes that could be reached and

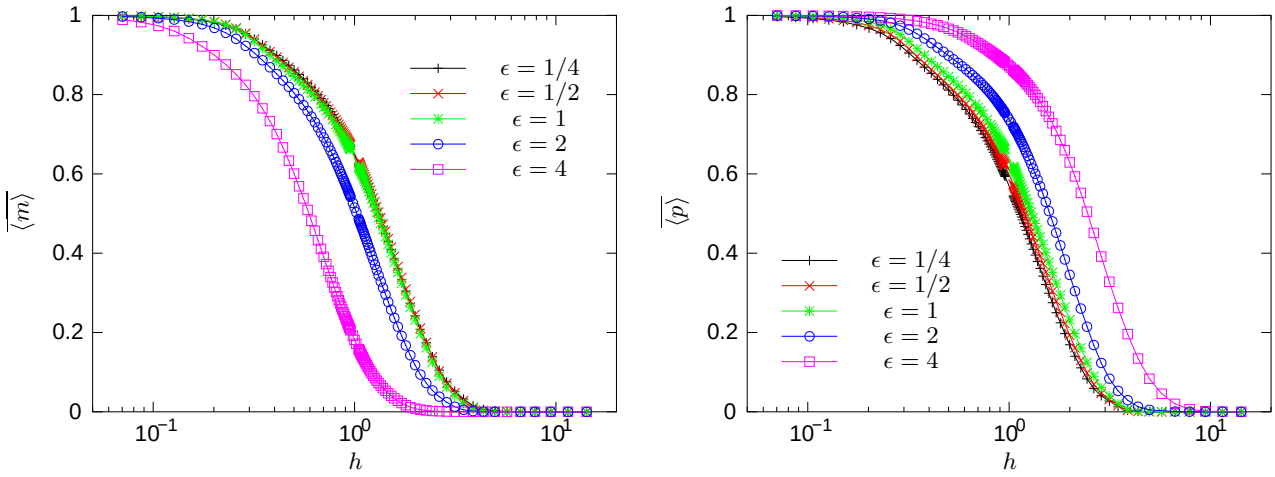

Fig. 1. Magnetization (left) and polarization (right) of the random quantum Ashkin-Teller chain versus the transverse field h. The different curves correspond to different values of $\epsilon = K_i/J_i$. The lattice size is $L = 12$.

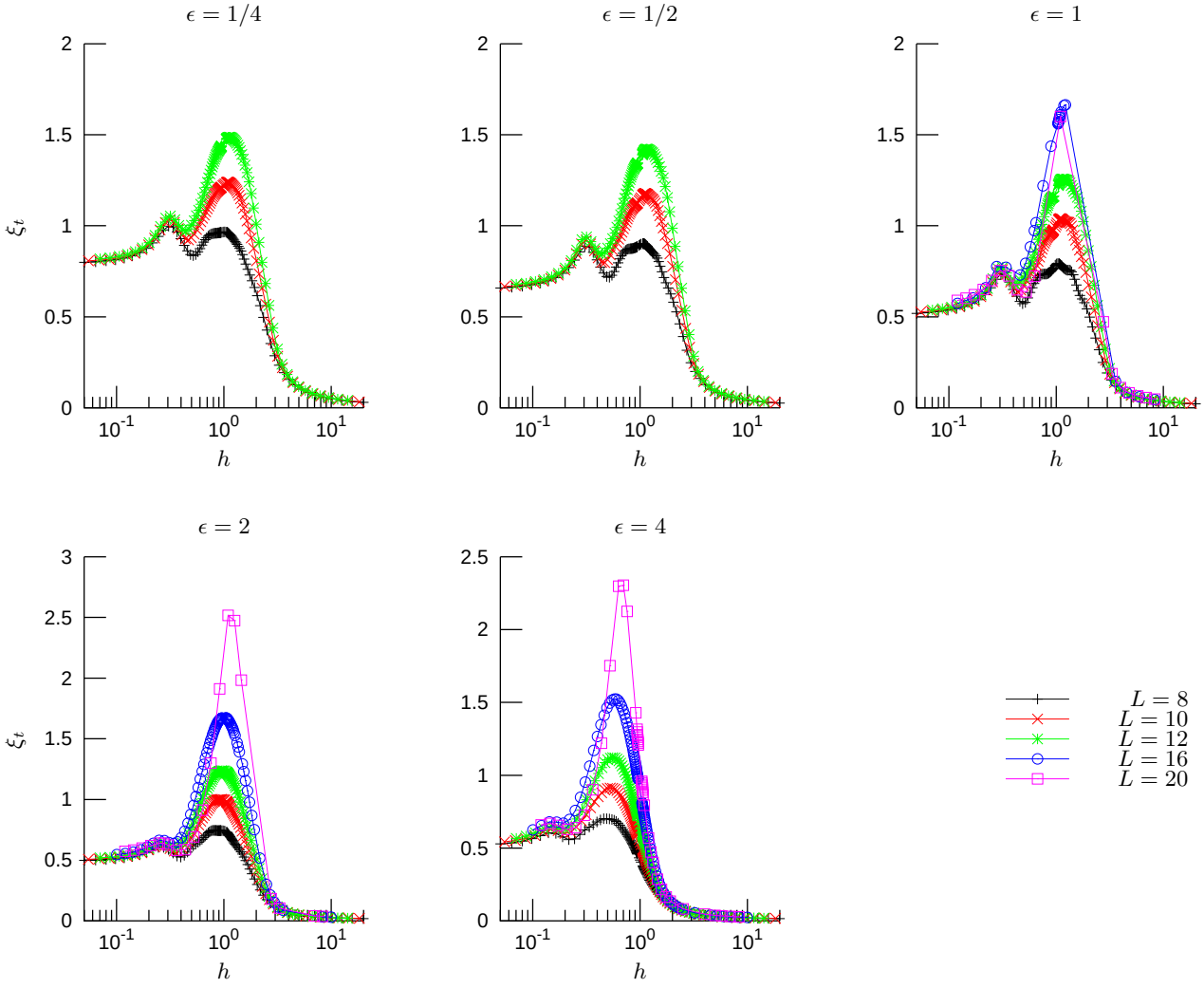

Fig. 2. Autocorrelation time ξ_t estimated by integration of the average spin-spin autocorrelation function $A_\sigma(t)$. The different graphs correspond to different values of ϵ and the different curves to different lattice sizes L.

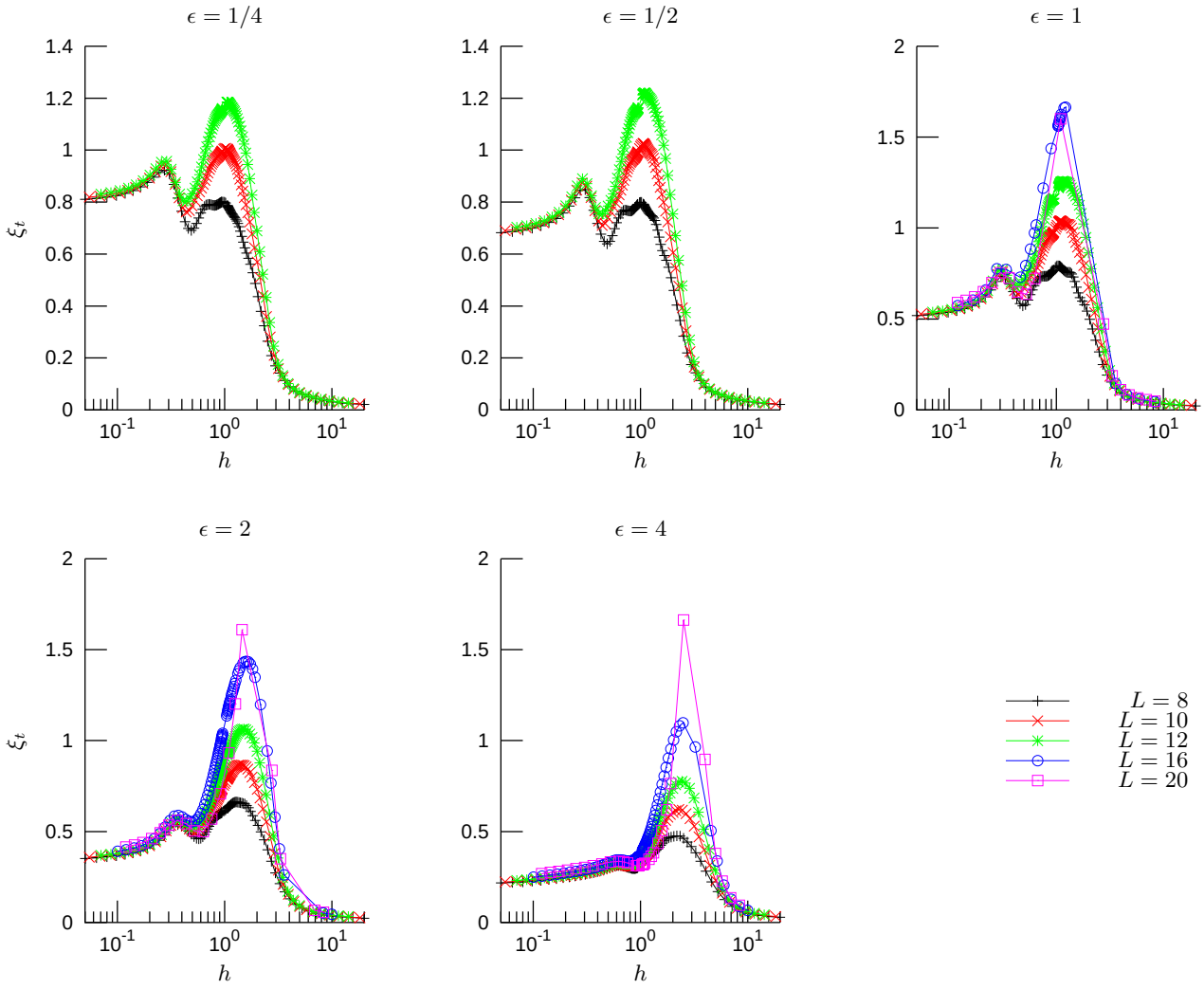

Fig. 3. Autocorrelation time ξ_t estimated by integration of the average polarization-polarization autocorrelation function $A_{\sigma\tau}(t)$. The different graphs correspond to different values of ϵ and the different curves to different lattice sizes L.

of the boundary magnetic and electric fields which favor a Baxter phase and therefore shift the whole phase diagram.

We also considered the first moment

$$\int_0^{+\infty} t\,\overline{A(t)}dt \;/\; \int_0^{+\infty} \overline{A(t)}dt \qquad (20)$$

that should be equal to the autocorrelation time ξ_t if the connected autocorrelation function $\overline{A(t)}$ displays a purely exponential decay $\overline{A(t)} \sim e^{-t/\xi_t}$. Like the autocorrelation time, the first moment was computed for both spin-spin and polarization-polarization autocorrelation functions. When plotted with respect to the transverse fields, two peaks are observed. Even though the shape of these peaks is not strictly identical to that of the autocorrelation time (19), in particular the second peak is higher and slightly broader, both quantities behave in the same way with the transverse field h. Therefore, the same conclusions can be drawn. A reconstructed phase diagram is shown on figure 4. It is qualitatively similar to the one presented in Ref. [31]. However, it is not symmetric under the transformation $\delta \leftrightarrow -\delta$. As discussed above, finite-size effects are here strengthened by the boundary magnetic and electric fields that globally shift the phase diagram.

3.2 Disorder fluctuations

In a random system, any thermodynamic average $\overline{\langle X \rangle}$ is the result of a quantum average

$$\langle X \rangle = \langle \psi_0[J_i, K_i] | X | \psi_0[J_i, K_i] \rangle \qquad (21)$$

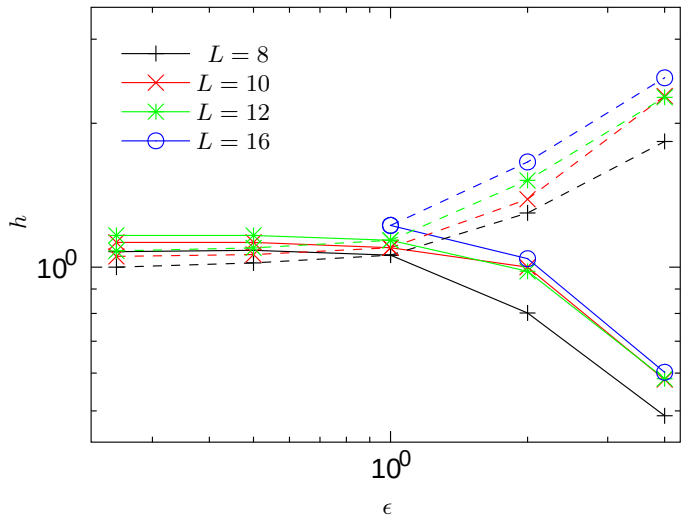

Fig. 4. Phase diagram in the parameter space (ϵ, h) obtained from spin-spin (continuous lines) and polarization-polarization (dashed lines) first moment (20). The different curves correspond to different lattice sizes.

followed by an average over coupling configurations

$$\overline{\langle X\rangle} = \int \langle\psi_0[J_i,K_i]|X|\psi_0[J_i,K_i]\rangle \wp(\{J_i,K_i\}) \prod_i dJ_i dK_i \tag{22}$$

where $|\psi_0[J_i,K_i]\rangle$ is the ground state of the system for a given coupling configuration $\{J_i,K_i\}$ and $\wp(\{J_i,K_i\})$ the probability of this configuration. At an IRFP, disorder fluctuations dominate over quantum fluctuations. The strength of the former can be measured by the variance

$$V_X = \overline{\langle X\rangle^2} - \overline{\langle X\rangle}^2. \tag{23}$$

We computed this quantity for both magnetization (V_σ) and polarization ($V_{\sigma\tau}$). As can be seen on figures 5 and 6, the variances V_σ and $V_{\sigma\tau}$ are numerically very stable. They vanish at high and low transverse fields h and display a well-defined single peak. In particular, there is no second peak at $h \sim J_2$. The locations of the maxima of the peaks are accurately determined and are in agreement with the ones estimated from autocorrelation times. The same conclusions can be drawn: the magnetic and electric transitions occur at very close control parameters δ, probably the same, for $\epsilon \leq 1$, while a finite shift is observed for $\epsilon > 1$. Even though only a weak dependence on the lattice size L of V_σ and $V_{\sigma\tau}$ is observed on figures 5 and 6, a systematic finite-size shift is present. For $\epsilon \leq 1$, the distance between the two critical lines decreases when the lattice size L increases, in agreement with the prediction of a unique transition. The coincidence of the maxima of the autocorrelation times with those of the disorder fluctuations shows that the phase transition is induced by disorder fluctuations, rather than quantum fluctuations, as expected at an IRFP.

As can be noticed on figures 5 and 6, the height of the peaks of the variance of disorder fluctuations increases slightly with the lattice size, at least for $L \leq 16$. The data for the lattice size $L = 20$ display indeed a smaller peak. This lattice size is the only one for which the average has not been computed over all possible disorder configurations but only over a subset ($\sim 10\%$) of them. The smaller peak for $L = 20$ is therefore probably due to an under-sampling of the dominant configurations at the critical point. 50,000 is still, at least for certain quantities, a too small number of disorder configurations. In the following, data for $L = 20$ should be taken with more care than smaller lattice sizes, for which an exact average over disorder was performed.

3.3 Entanglement entropy

When the degrees of freedom of the system can be divided into two subsets A and B, and therefore when the Hilbert space can be decomposed as a tensor product $\mathcal{H} = \mathcal{H}_A \otimes \mathcal{H}_B$, the degree of entanglement of the two sub-blocks is conveniently measured by the von Neumann entanglement entropy of A with the rest of the system [37]:

$$S_A = -\mathrm{Tr}_{\mathcal{H}_A} \rho_A \log \rho_A \tag{24}$$

where ρ_A is the reduced density matrix

$$\rho_A = \mathrm{Tr}_{\mathcal{H}_B} \rho \tag{25}$$

and ρ the density matrix of the full system. In the case of a pure state $|\psi\rangle$, the latter is the projector $\rho = |\psi\rangle\langle\psi|$. In the following, we will consider the subset A made of the ℓ spins at the left of the chain.

Entanglement entropy has recently attracted a lot of attention because of Conformal Field Theory (CFT) predictions at pure critical points [38,39]. The predicted logarithmic behavior with ℓ is also observed in RTFIM but with a prefactor that involves an effective central charge $\tilde{c} = \frac{1}{2}\ln 2$ [40]. The entanglement entropy is also commonly used in the literature to determine phase boundaries [37]. Indeed, it is expected to be larger when quantum correlation functions are long-range. At an IRFP, the entanglement entropy is related to the probability of a strongly correlated cluster across the boundary between the two blocks A and B. Numerically, the reduced density matrix ρ_A being computed and diagonalized at each step of the DMRG algorithm, the entanglement entropy is given without any additional computational effort.

The average entanglement entropy $\overline{S(\ell)}$ of the random quantum Ashkin-Teller chain is plotted on figure 7 for $\ell = L/2$. For $\epsilon = 4$, two peaks can be observed and interpreted as the signature of the two phase transitions. As expected, one single peak is present when $\epsilon \leq 1$. However, only one peak can be distinguished in the case $\epsilon = 2$, while autocorrelation time indicates the existence of two transitions. Because of the finite-size of the system, the expected two peaks are probably merged into a single one. This scenario is compatible with what is observed for $\epsilon = 4$: what was only a shouldering at the left of the peak for $L = 8$ becomes a second independent peak at $L = 20$.

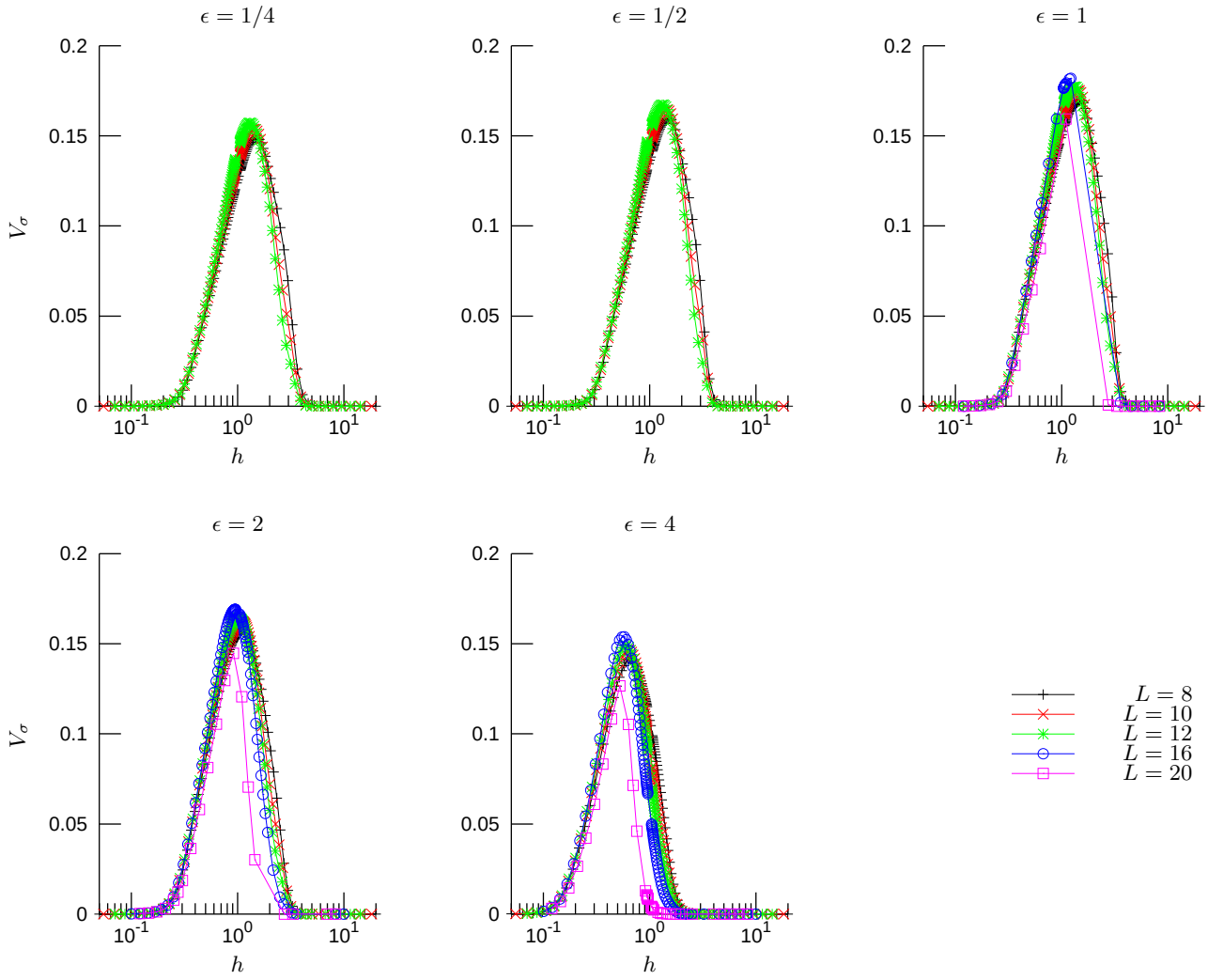

Fig. 5. Variance of disorder fluctuations of magnetization. The different graphs correspond to different values of ϵ and the different curves to different lattice sizes L.

The phase diagram is qualitatively the same as previously constructed. However, the two peaks are not located at the same position as those displayed by the integrated autocorrelation times, or the variance of disorder fluctuations. At $\epsilon = 4$, they are instead found at $\delta_c \sim -0.10$ and $\delta_c \sim -1.33$, far from the estimates $\delta_c \simeq 0.54$ and -0.99. This large difference is probably due to Finite-Size effects. Indeed, magnetization, polarization and autocorrelation functions were computed at the center of the lattice, i.e. at the site $L/2$. In contrast, the entanglement entropy is a global quantity, therefore more sensitive to the presence of boundary fields.

CFT predicts that the entanglement entropy of a block of size ℓ behaves as [39]

$$S(\ell) = \rho c \ln \left[\frac{L}{\pi a} \sin \frac{\pi \ell}{L} \right] + \text{Cst.}, \qquad (26)$$

where c is the central charge and ρ is equal to $1/3$ for periodic boundary conditions and $1/6$ for open boundaries. However, this relation was obtained on a finite but continuous manifold and not on a lattice. Therefore, it is only poorly verified by our numerical data, for which strong lattice effects are still present. Nevertheless, the predicted dependence on the lattice size L is well reproduced by the numerical data. For an equal partition of the system, i.e. when plugging $\ell = L/2$ into (26), the entanglement entropy $S(L/2)$ is expected to be a linear function of $\ln L$ with a slope ρc. The numerical data at the maximum of $S(L/2)$ is in good agreement with this prediction as shown on figure 8. This confirms the divergence of the correlation length as the lattice size and therefore, the occurrence of a phase transition. Because of the magnetic and electric fields coupled to the boundaries of the system during

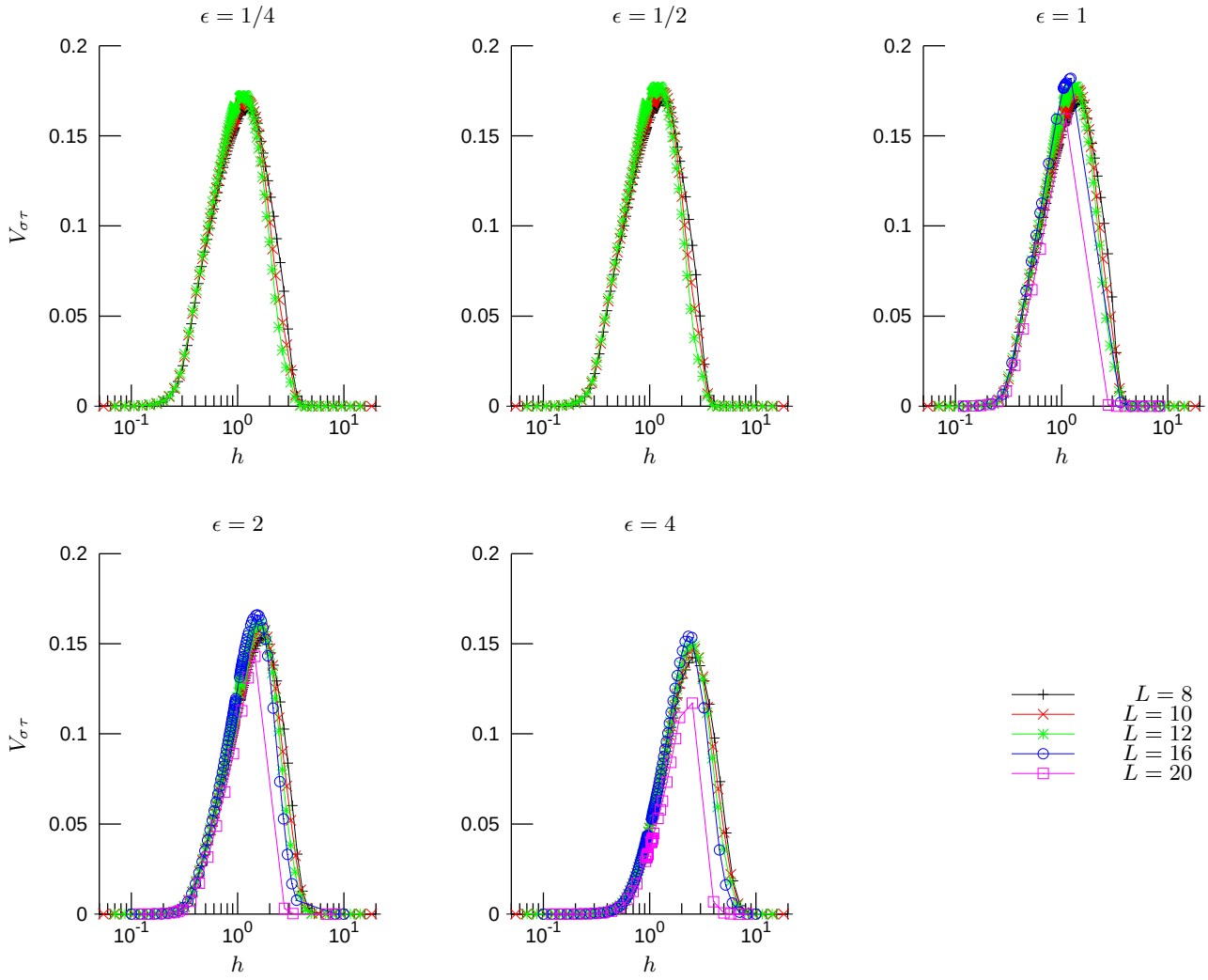

Fig. 6. Variance of disorder fluctuations of polarization. The different graphs correspond to different values of ϵ and the different curves to different lattice sizes L.

the numerical computations, the CFT predictions for the slope of $S(L/2)$ with $\ln L$ do not apply.

4 Autocorrelation functions

As discussed in the introduction, the average connected autocorrelation functions $\overline{A(t)}$ display three different behaviors according to the values of the parameters δ and ϵ, i.e. the position in the phase diagram. On the critical lines, a slow relaxation (3) depending on the logarithm of t is expected. In the Griffiths phases, rare regions induce an algebraic decay (2) of the autocorrelation functions, with an exponent $1/z$. Finally, away from the Griffiths phases, a more usual exponential decay is recovered.

The algebraic decay of autocorrelation functions in the Griffiths phases has been observed numerically in the case of the random quantum Ising chain by exploiting the mapping onto a gas of free fermions [14]. The lattice sizes that we were able to reach with DMRG being much smaller, such an algebraic decay of the spin-spin or polarization-polarization autocorrelation functions could not be observed for the random Ashkin-Teller model. A purely algebraic behavior is indeed expected to hold only in the large-time limit $t \gg 1$ and in the thermodynamic limit $L \gg 1$. A transient regime may be observed for small times t while, for large times t, the finite-size of the system may induce an exponential decay of autocorrelation functions. Usually, one looks for an intermediate regime in the numerical data where the asymptotic behavior holds. No such intermediate regime could be found for both the spin-spin or polarization-polarization autocorrelation functions. This is particularly clear when plotting an effective exponent $\frac{d \ln \overline{A(t)}}{d \ln t}$ versus t. For values of the transverse field h ex-

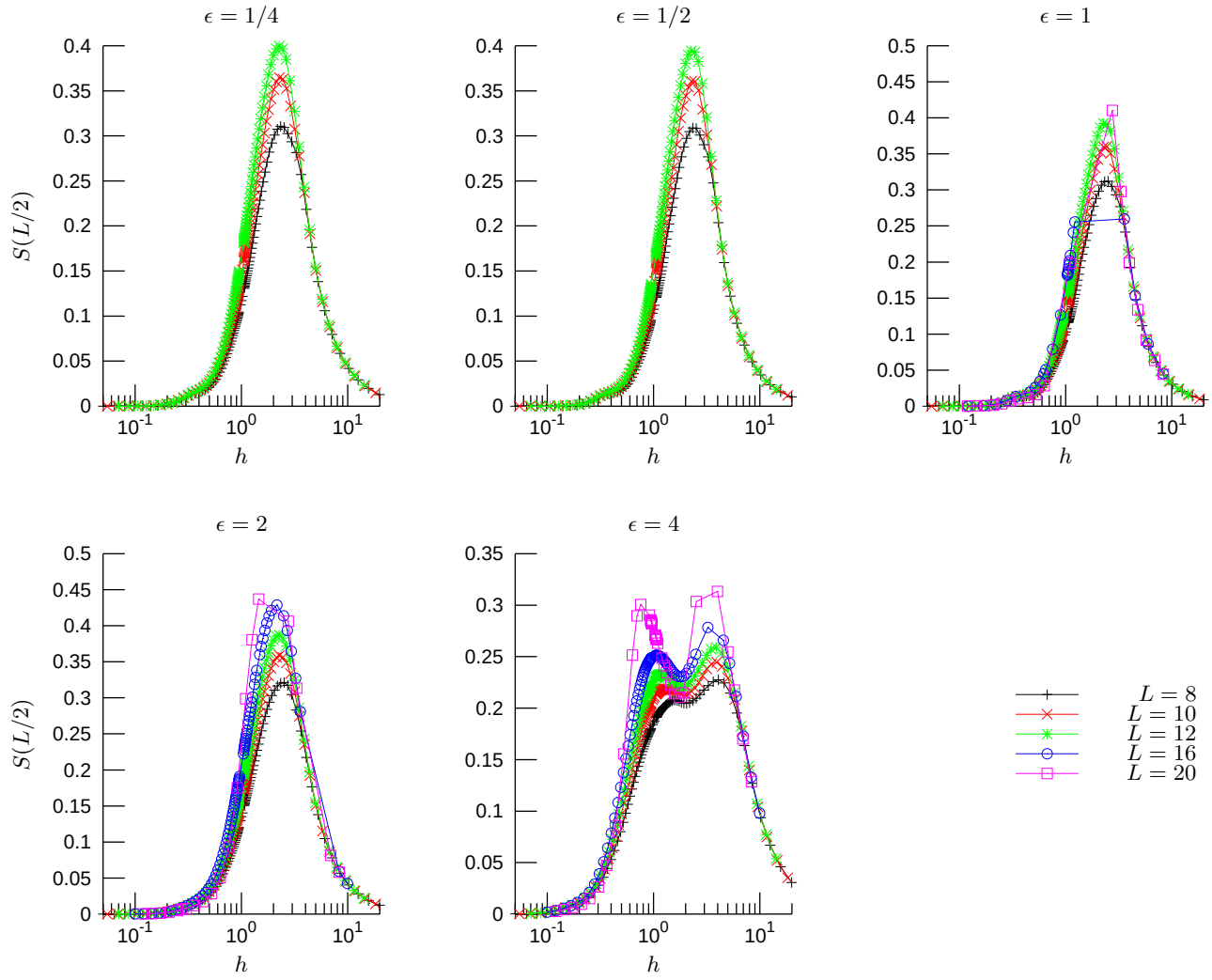

Fig. 7. Entanglement entropy for an equal partition of the system, i.e. $\ell = L/2$. The different graphs correspond to different values of ϵ and the different curves to different lattice sizes L.

pected to be in the Griffiths phases, two non-algebraic regimes, where the effective exponent varies with t, are observed at short and large times. But in between, no plateau corresponding to a purely algebraic decay could be distinguished.

To fit our numerical data, we used an extended expression of the one proposed by Rieger *et al.* for autocorrelation functions in a Griffiths phase [11]. The assumptions are the same: in the paramagnetic phase, the probability of an ordered region of linear size ℓ scales as $\wp(\ell) \sim e^{-c\ell}$ and its tunneling time is $\tau(\ell) \sim e^{\sigma'\ell}$. In a finite system of width L, the linear size of rare regions is bounded by L so the average autocorrelation function reads

$$\begin{aligned}\overline{A(t)} = \overline{e^{-t/\tau}} &= \int_0^L \wp(\ell) e^{-t/\tau(\ell)} d\ell \\ &= \frac{t^{-c/\sigma'}}{\sigma'} \int_{te^{-\sigma' L}}^{t} v^{c/\sigma'-1} e^{-v} dv \\ &= \frac{t^{-1/z}}{\sigma'} \left[\gamma(1/z, t) - \gamma(1/z, te^{-\sigma' L})\right] \quad (27)\end{aligned}$$

where $v = te^{-\sigma'\ell}$, $\sigma'/c = z$ is the dynamical exponent, and $\gamma(a, x)$ is the incomplete gamma function. In the limit of large time t and lattice size L, one recovers the prediction $\overline{A(t)} = \frac{\Gamma(1/z)}{\sigma'} t^{-1/z}$ obtained in the saddle-point approximation.

The numerical estimates of the connected autocorrelation functions were fitted with the 4-parameter non-linear

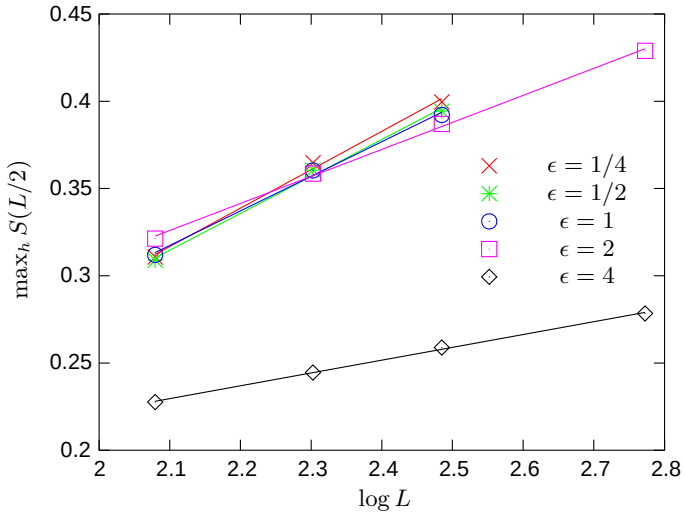

Fig. 8. Scaling of the maximum of the entanglement entropy $S(L/2)$ for an equal partition of the system, i.e. $\ell = L/2$, with the logarithm of the lattice size. The different symbols correspond to different values of ϵ and the straight lines are linear fit of the data.

ansatz

$$\overline{A(t)} = a_1 t^{-a_2} |\gamma(a_2, a_3 t) - \gamma(a_2, a_4 t)|. \qquad (28)$$

The bounds $0 < a_2 \leq 1$ were imposed during the fitting procedure. The quality of the fit was quantified using the mean-square deviation χ^2. Because the boundaries of the Griffiths phases are not known with a good accuracy, the data were also fitted with an exponential $\overline{A(t)} = a_1 e^{-a_2 t}$. Spin-spin and polarization-polarization autocorrelation functions are plotted respectively on figures 9 for various transverse fields h at $\epsilon = 4$. The continuous lines correspond to the best fit, Eq. (28) or exponential, i.e. the one with the smallest mean square deviation χ^2. The inverse $1/z$ of the dynamical exponent is indicated in the legend when (28) is the best fit, while *exp* indicates a fit with an exponential. As can be seen on the figures, the data are nicely reproduced by an exponential decay for large and small transverse fields h. Close to the transition point, the best fit is obtained with (28), which means that the corresponding range of transverse fields is in a Griffiths phase. As expected, when $\epsilon \leq 1$, these phases are centered around $h = 1$ and their boundaries are similar for spin-spin and polarization-polarization autocorrelation functions. For $\epsilon = 4$, the Griffiths phase is shifted to smaller values of the transverse field for spin-spin autocorrelation functions and to larger ones for polarization-polarization autocorrelations. For $\epsilon = 2$, the shift is seen only for the polarization-polarization autocorrelation functions. It was also the case for the peak of the autocorrelation time (figure 2). At the boundaries of the Griffiths phases, the data is not well fitted, neither by an exponential form nor by the *ansatz* (28). When the best fit is obtained with the *ansatz* (28), the dynamical exponent takes a value $z = 1$, i.e. saturating the imposed bound $z \leq 1$. The deviation between the fit and the numerical data is clearly visible on figures 9. The transverse fields for which such a deviation occurs, are probably in a region of cross-over where the autocorrelation functions display a more complex behavior.

On figures 10 and 11, the inverse of the dynamical exponents z is plotted versus the transverse field h. As conjectured in Ref. [31], the dynamical exponents display a peak centered at the corresponding critical point, i.e. at the magnetic transition for the dynamical exponent of spin-spin autocorrelation functions and electric transition for polarization-polarization autocorrelations. As already observed for other peaked quantities, the two transitions occur at the same control parameters for $\epsilon \leq 1$ and are separated for $\epsilon > 1$. Note that the maxima of the dynamical exponents are found at the locations of those of the autocorrelation times and of the variance of disorder fluctuations. Between these two transitions lines, there is therefore a double Griffiths phase, i.e. a disordered Griffiths phase in the magnetic sector and an ordered one in the electric sector where both dynamical exponents z are larger than 1. However, as seen on figures 10 and 11, these Griffiths phase are not infinite but have a finite extension, because of the binary distribution of the couplings J_i and K_i. For $\epsilon = 4$, it is observed that the magnetic and electric Griffiths phases still overlap. Nevertheless, it will probably not be the case anymore for larger values of ϵ.

In the random Ising chain, the dynamical exponent was shown to behave as $z \sim 1/2|\delta|$ in the Griffiths phase [41]. A similar behavior seems to be also reasonable in the case of the random Ashkin-Teller chain, as can be seen on figures 10 and 11. The boundaries $\delta_+ = -\ln h_+$ and $\delta_- = -\ln h_-$ of the Griffiths phase were first estimated respectively as the first and last points with a dynamical exponent $z > 1$. The critical point is assumed to be located at $\delta_c = (\delta_+ + \delta_-)/2$. The two dashed lines plotted on figures 10 and 11 simply correspond to straight lines $1/z(\delta) = (\delta - \delta_c)/(\delta_+ - \delta_c)$ for $\delta \in [\delta_c; \delta_+]$ and $1/z(\delta) = (\delta - \delta_c)/(\delta_- - \delta_c)$ for $\delta \in [\delta_-; \delta_c]$. The slope is not equal to two, as in the Ising model, but is in the range $1-1.5$. As the lattice size is increased, the numerical data seem to accumulate on these straight lines, at least at the boundaries of the Griffiths phase. In the neighborhood of the critical point, much larger lattice sizes would be necessary to test this linear behavior of $1/z$. In the case of $L = 20$, the dynamical exponent seems to be overestimated for $h < h_c$. Again, this may be explained by the under-sampling already observed with disorder fluctuations of magnetization and polarization.

5 Conclusions

The random quantum Ashkin-Teller chain has been studied by means of time-dependent Density Matrix Renormalization Group. The average over all possible disorder configurations was performed for $L \leq 16$. For $L = 20$, a partial average is observed to induce an under-sampling of disorder fluctuations of magnetization and polarization. Such partial averages are commonly used in the literature

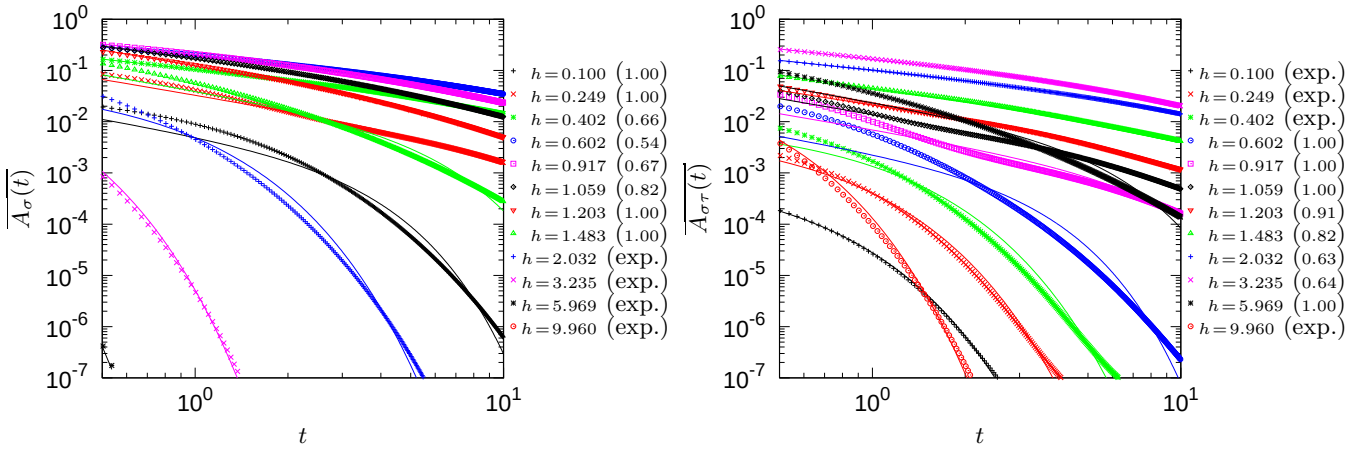

Fig. 9. Spin-spin (left) and polarization-polarization (right) autocorrelation functions of the random quantum Ashkin-Teller chain versus time t. The different graphs correspond to different values of the transverse field h. The continuous lines correspond to a fit, either with the *ansatz* (28) or with an exponential. In the legend, the number between parenthesis after the transverse field h is the estimate of $1/z$ given by the fit. When the best fit is the exponential, *exp* is indicated instead.

in the study of random systems. Our data show that they should be considered with great care, especially in the quantum case.

The analysis of integrated autocorrelation times and of the variance of disorder fluctuations leads to a phase diagram qualitatively in agreement with the one conjectured by Hrahsheh *et al.* on the basis of SDRG [31]. However, finite-size effects are large, especially for entanglement entropy, and our lattice sizes are too small to allow for an accurate extrapolation in the thermodynamic limit. The coincidence of the maxima of disorder fluctuations with the critical lines confirms that the phase transition is governed by disorder fluctuations, and not by quantum fluctuations. Nevertheless, the divergence of the entanglement entropy as the logarithm of the lattice size is recovered, as in pure quantum chains. In the regime $\epsilon > 1$, the existence of a double Griffiths phase is confirmed. Using an original method to take into account finite-size effects, the two dynamical exponents, associated to the algebraic decay of spin-spin and polarization-polarization autocorrelation functions respectively, could be computed. They display the expected behavior in a Griffiths phase: a peak centered at the magnetic or electric transition. Furthemore, it seems reasonnable to assume that they diverge in the thermodynamic limit as $z(\delta) \sim 1/|\delta|$.

It is our pleasure to gratefully thank Cécile Monthus for discussions and for having pointing out some useful references on the topic.

References

1. A.B. Harris (1974) *J. Phys. C: Solid State Phys.* **7** 1671.
2. S. Wiseman, and E. Domany (1995) *Phys. Rev. E* **51** 3074.
3. J. Cardy, and J.L. Jacobsen (1997) *Phys. Rev. Lett.* **79**, 4063.
4. J. L. Jacobsen and J. L. Cardy (1998) *Nucl. Phys. B* **515**, 701.
5. B.M. McCoy and T.T. Wu (1968) *Phys. Rev.* **176** 631.
6. B.M. McCoy et T.T. Wu (1969) *Phys. Rev.* **188** 982.
7. R.B. Griffiths (1969) *Phys. Rev. Lett.* **23** 17.
8. T. Vojta (2006) *J. Phys. A: Math. Gen.* **39** R143.
9. C. Chatelain (2013) *Europhys. Lett.* **102** 66007.
10. C. Chatelain (2014) *Phys. Rev. E* **89** 032105.
11. H. Rieger, and A. P. Young. (1997) *Quantum Spin Glasses.* In Complex Behaviour of Glassy Systems, Eds by Miguel Rub and Conrado Prez-Vicente, Lecture Notes in Physics 492. Springer Berlin Heidelberg.
12. T.D. Schultz, D.C. Mattis, and E.H. Lieb (1964) *Rev. Mod. Phys.* **36** 856.
13. R. Shankar, and G. Murthy (1987) *Phys. Rev. B* **36** 536.
14. A.P. Young, and H. Rieger (1996) *Phys. Rev. B* **53**, 8486.
15. C. Dasgupta, and S.-K. Ma. (1980) *Phys. Rev. B* **22** 1305.
16. D.S. Fisher (1992) *Phys. Rev. Lett.* **69** 534.
17. D.S. Fisher (1995) *Phys. Rev. B* **51** 6411.
18. F. Iglói, and C. Monthus (2005) *Phys. Rep.* **412** 277.
19. F. Iglói, and H. Rieger (1998) *Phys. Rev. B* **57** 11404.
20. I. Kovács, and F. Iglói (2010) *Phys. Rev. B* **82** 054437.
21. I. Kovács, and F. Iglói (2011) *Phys. Rev. B* **83** 174207.
22. I. Kovács, and F. Iglói (2012) *Eur. Phys. Lett.* **97** 67009.
23. T. Senthil and S. N. Majumdar (1996) *Phys. Rev. Lett.* **76**, 3001.
24. E. Carlon, C. Chatelain, and B. Berche (1999) *Phys. Rev. B* **60**, 12974.
25. J. Ashkin, and E. Teller (1943) *Phys. Rev.* **64**, 178.
26. C. Fan (1972) *Phys. Lett.* **39A**, 136.
27. M. Kohmoto, M. den Nijs, and L.P. Kadanoff (1981) *Phys. Rev. B* **24**, 5229.
28. C. Fan (1972) *Phys. Rev. B* **6** 902.
29. G. Kamieniarz, P. Kozłowski, and R. Dekeyser (1997) *Phys. Rev. E* **55**, 3724.
30. E. Carlon, P. Lajkó, and F. Iglói (2001) *Phys. Rev. Lett.* **87** 277201.

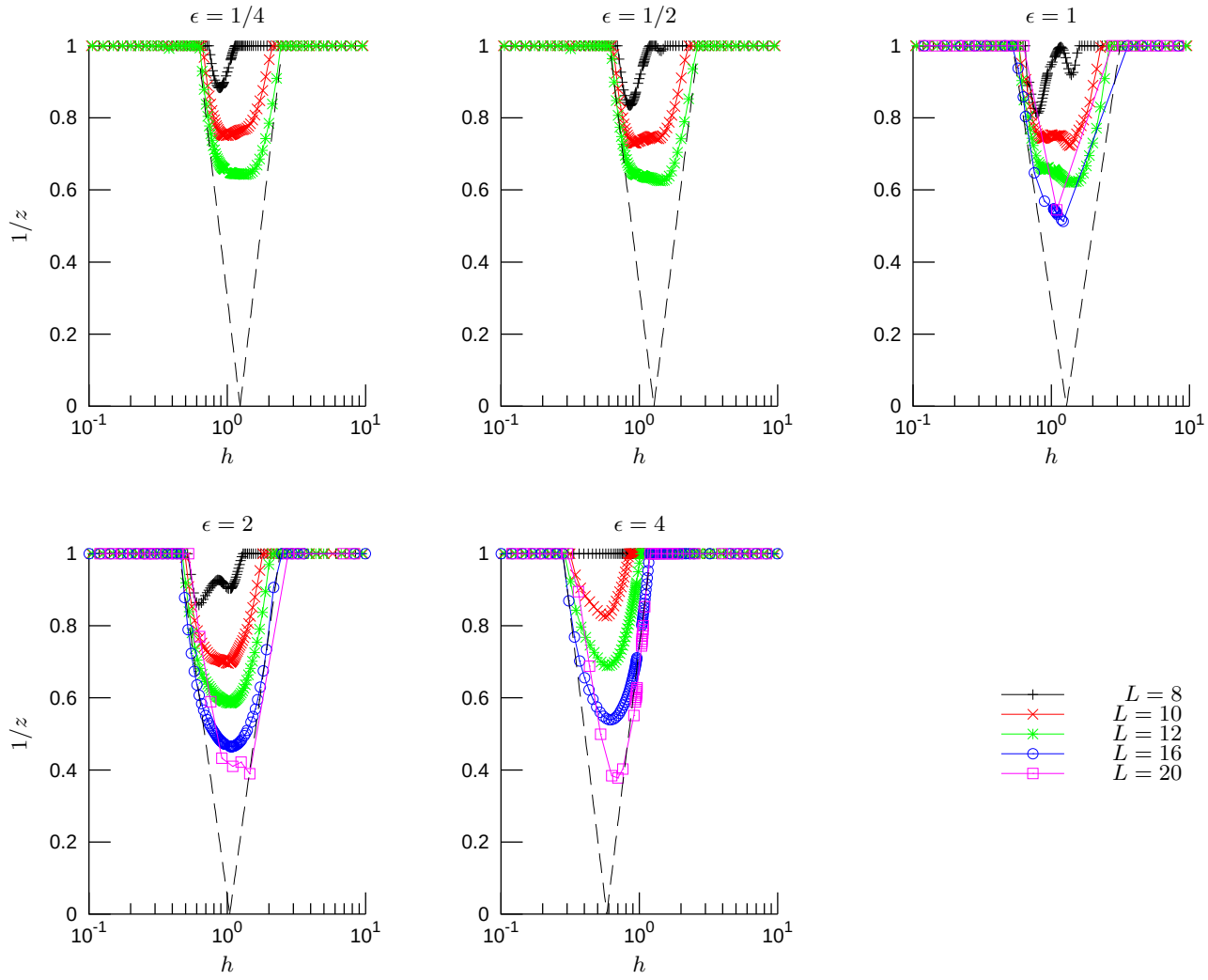

Fig. 10. Inverse of the dynamical exponent z estimated by a fit of the spin-spin autocorrelation functions with Eq. (28) and plotted versus the transverse field h. The different curves correspond to different lattice sizes and the different graphs to different values of ϵ.

31. F. Hrahsheh, R. Narayanan, J.A. Hoyos, and T. Vojta (2014) *Phys. Rev. B* **89** 014401.
32. F. Hrahsheh, J.A. Hoyos, and T. Vojta (2012) *Phys. Rev. B* **86** 214204.
33. B. Derrida, and H. Hilhorst (1981) *J. Phys. C: Solid State Phys.* **14** L539.
34. S.R. White (1992) *Phys. Rev. Lett.* **69** 2863.
35. S.R. White (1993) *Phys. Rev. B* **48** 10345.
36. U. Schollwoeck (2005) *Rev. Mod. Phys.* **77** 259.
37. L. Amico, R. Fazio, A. Osterloh, and V. Vedral (2008) *Rev. Mod. Phys.* **80**, 517.
38. G. Vidal, J.I. Latorre, E. Rico, and A. Kitaev (2003) *Phys. Rev. Lett.* **90**, 227902.
39. P. Calabrese and J. Cardy (2004) *J. Stat. Mech.: Theory Exp.* P06002.
40. G. Refael and J.E. Moore (2004) *Phys. Rev. Lett.* **93**, 260602.
41. F. Iglói, R. Juhász, and P. Lajkó (2001) *Phys. Rev. Lett.* **86** 1343

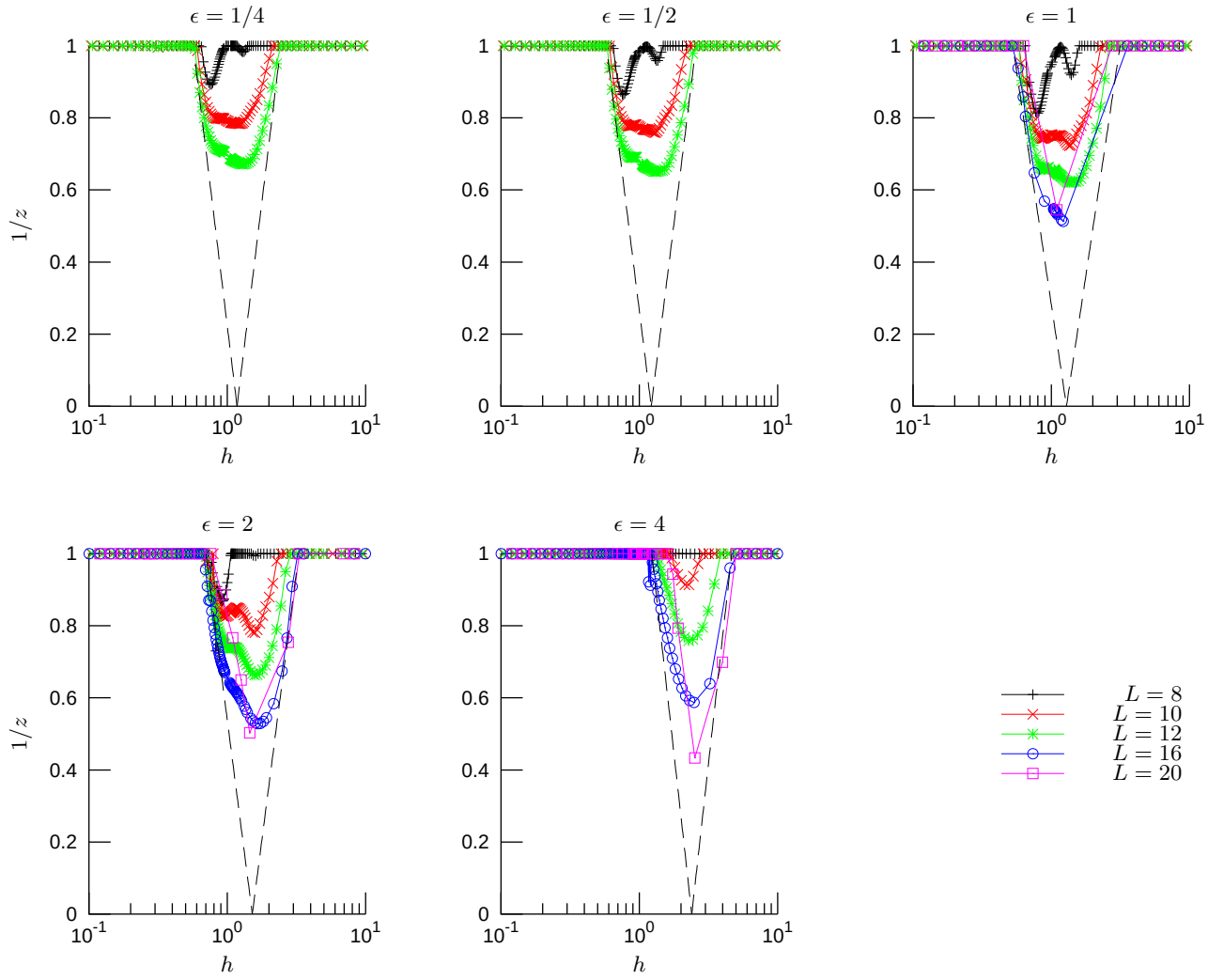

Fig. 11. Inverse of the dynamical exponent z estimated by a fit of the polarization-polarization autocorrelation function with Eq. (28) and plotted versus h. The different curves correspond to different lattice sizes and the different graphs to different values of ϵ.